

## Experimental Evaluation of the Effect of Flow Deflectors on Helicopter Rotor Wake Vortices

K. Bourne<sup>1</sup>, P. Manovski<sup>2</sup>, K.R. Reddy<sup>1</sup> and A. Ooi<sup>3</sup>

<sup>1</sup>Air Operations Division

DSTO Melbourne, Fishermans Bend 3207, Australia

<sup>2</sup>Air Vehicles Division

DSTO Melbourne, Fishermans Bend 3207, Australia

<sup>3</sup>Department of Mechanical Engineering

The University of Melbourne, Melbourne 3010, Australia

### Abstract

Understanding the rotor wake flow characteristics of a helicopter is fundamental to the investigation of its aerodynamic characteristics. When operating close to the ground the rotor wake can reflect to create large, doughnut-shaped vortices around the helicopter. In certain environments these vortices can cause the formation of dust clouds, resulting in a phenomenon commonly referred to as *brownout*. This study seeks to assess the interactional aerodynamics between a small-scale rotor wake and a range of active and passive flow deflectors. Two sets of experimental results will be presented, the first a smoke flow visualisation which qualitatively assessed the potential of both passive and active deflectors to modify major wake structures. The second experiment used Particle Image Velocimetry (PIV) to assess the effect of the active deflectors.

### Introduction

#### Brownout

The rotor wake flow characteristics associated with helicopter operations in level and vertical flight are reasonably well understood, but this does not extend to phenomena associated with aerodynamic interference effects. The interaction between the main rotor wake and external objects, such as buildings, ship structures and ground planes, as well as impingement of the rotor downwash on airframe components, are highly complex flow conditions. In particular, the disturbance of sand and dust particles by the rotor wake during low altitude, low speed flight and hover leads to significant operational difficulty.

Brownout is a complex aerodynamic environment characterised by the entrainment of small ground particles through the rotor [2, 4, 8, 10]. When brownout conditions are fully developed, cockpit visibility is fully obscured by the dust particles entrained by the helicopter rotor wake. In such instances aircrew can rapidly lose situational awareness, significantly increasing the probability of a mishap. Despite considerable research efforts, an effective solution to enable safe operations in brownout conditions has not yet been developed.

Brownout may be considered a phenomenon comprising the flow structure of a helicopter rotor wake as well as the motion of particles. The flow structure will depend on the helicopter flight characteristics and its proximity to the ground, whereas the particle motion will depend on the size, shape and mass of the particles in question.

This study seeks to experimentally investigate the aerodynamic flow structures created by a helicopter rotor In Ground Effect (IGE) and how they may be influenced by flow-altering devices.

Although the motivation for this research is to investigate aerodynamic methods by which brownout may be mitigated, a thorough understanding of the fundamental flow field is the prime concern. An assessment of the effect that dust particles themselves may have on the rotor wake is considered beyond the scope of this study. To this end, it is assumed the motion of dust particles will follow the motion of the air without altering the flow structure. It is acknowledged that such an assumption will not always be valid, particularly in a sandy environment.

#### Ground Effect

All testing took place with the rotor operating IGE. Brownout occurs most commonly when the helicopter is IGE, a flight regime defined as operations within a rotor height of one to two rotor diameters (D) from the ground. Ground effect restricts the airflow through the rotor and subsequently alters the geometry of the rotor wake [1, 3, 7].

#### Smoke Flow Visualisation

A sub-scale rotor rig based on previous experiments [11] was used to qualitatively investigate the effect of passive and active flow deflectors on the rotor wake. The intent of the deflectors was to push the rotor tip vortices further outboard, and by doing so potentially push the ground vortex produced by the rotor flow away from the central region of the rotor wake, where the cockpit is located.

To assess the effect of the deflectors, flow visualisation was undertaken using smoke. A rotor model was built and mounted in the working section of the Defence Science and Technology Organisation (DSTO) Low Speed Wind Tunnel (LSWT), which has an octagonal working section 2.74 m wide  $\times$  2.13 m high. A ground plane was installed above the model to ensure the rotor was operating IGE at 0.5D. The rotor radius was 640 mm and the blade collective pitch angle was set at 13°.

#### Flow Deflectors

Four deflectors were tested, three passive and one active. Each was fixed between the rotor and the ground plane as shown in figure 1. Due to the fact that the analysis was restricted to a qualitative assessment, the effect of the deflectors was measured by the change, if any, in the lateral deflection of the blade tip vortices. Detailed in figure 2 are the profiles of the passive deflectors, each chosen based on their potential to radially deflect the flow. The passive deflectors each had a radius of 600 mm, the largest feasible size with respect to the rotor radius. The active deflector, shown in figure 3, was constructed from two circular flat plates of 400 mm diameter, connected to a high-pressure compressed air supply. A small conical diffuser was placed at the

centre of the bottom plate to promote an evenly distributed radial flow.  $V_B$  refers to the airflow in the duct, and  $V_X$  indicates the resulting radial flow.  $V_X$  was measured using a handheld anemometer and found to be approximately 8 m/s at the outlet, dropping to 6 m/s at a radial distance of 50 mm, then decreasing by 1 m/s for every additional 50 mm. The separation distance between the deflectors and the ground plane was 225 mm.

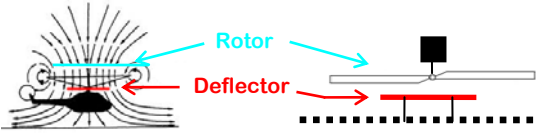


Figure 1. Experimental setup with reference to full-scale scenario.



Figure 2. Passive deflector profiles. (a) circular flat plate, (b) curved edge and (c) truncated cone.

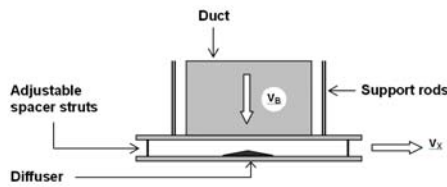


Figure 3. Active deflector.

Results showed that all passive deflectors produced very little change in the flow structure of the blade tip vortices. By way of example, figure 4 compares the baseline case with the results of the curved edge, passive deflector. There is very little discernable change to the trajectory of the blade tip vortices, which make up the dominant flow structure of the rotor wake.

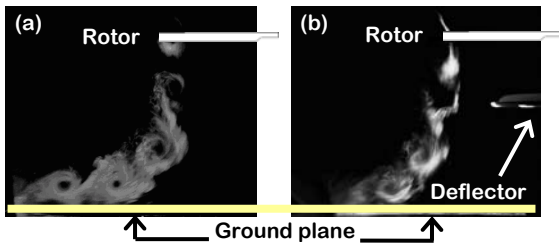


Figure 4. (a) Image of the baseline rotor wake flow visualisation, IGE. (b) Flow field with curved-edge passive deflector installed.

Shown in figure 5(a) is the blade tip vortex flow structure prior to the operation of the active deflector. The deflector is behaving like a passive deflector in this instance, with negligible effect on the dominant features of the rotor wake. Figure 5(b) shows the flow structure after the active deflector has been engaged. The alteration to the flow structure is evident, as emphasised by the overlay outlining the trajectory of the blade tip vortices. After activation of the deflector, the radial position of the blade tip vortices was increased, providing the desired effect.

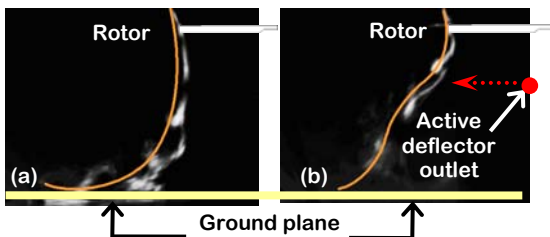


Figure 5. (a) Wake profile before deflector activated. (b) Flow field as altered by active deflector.

## Particle Image Velocimetry Measurements

### Experimental Setup and Data Processing

For the PIV measurements, the 2D plane of interest was illuminated using a New Wave Solo PIV 200XT Nd:YAG dual-pulse laser. The laser was mounted above the working section of the DSTO LSWT. Images were acquired using a TSI PowerView™ Plus CCD camera, fitted with a 200 mm Micro Nikkor f/4 lens. The camera was mounted orthogonally to the laser sheet, as shown in figure 6. Data acquisition and processing was achieved using the TSI INSIGHT™ 4G software.

The experiments were undertaken with a small-scale two-bladed rotor. The blade had no twist or camber and a radius ( $R$ ) of 110 mm. The collective pitch angle was fixed at  $30^\circ$  to maximise the rotor thrust and generate the maximum downwash. The deflector, detailed in figure 7, was attached to the ground plane beneath the rotor. A Hall-Effect sensor was mounted to the rotor shaft and used to trigger the PIV data acquisition at a blade azimuth angle of  $90^\circ$ , to ensure the blade was clear of the recorded image. The maximum acquisition rate of the equipment (2 Hz) was below the nominal operational speed of the rotor (30 Hz), and as such the results could be phase-averaged but not time-averaged.

The PIV seed particles were DEHS (Di-2-EthylHexyl-Sebacate) droplets generated using a Laskin nozzle. Given only the hover condition was being examined, and therefore no wind tunnel operation was required, the working section was isolated from the rest of the LSWT.

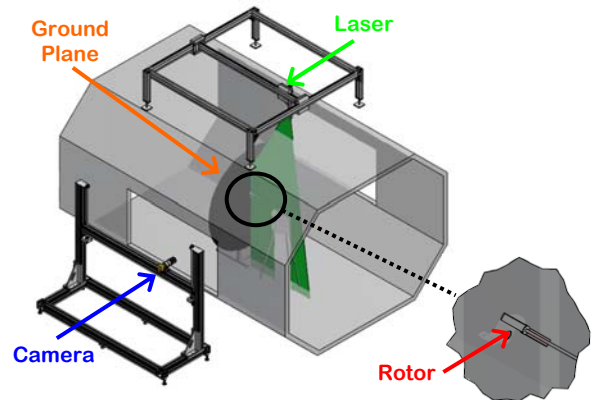


Figure 6. PIV setup showing the rotor assembly installed in the LSWT, with cameras positioned orthogonal to the laser sheet.

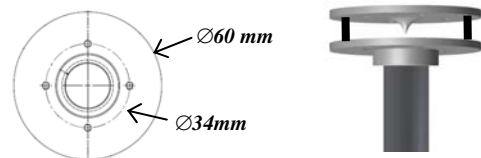


Figure 7. Detail of active deflector used for PIV experiments.

The offset distance to the PIV camera with the rotor aligned to the tunnel centreline was approximately 1.4 m, which resulted in a reproduction ratio of 6.7 and a spatial resolution of  $60.3 \mu\text{m}/\text{pixel}$ . For test cases with a plan view, the reproduction ratio was 5.9, with a spatial resolution of  $52.85 \mu\text{m}/\text{pixel}$ . Based on the requirement that the maximum particle displacement be less than 25% of the initial interrogation window (IW) size of  $64 \times 64$  pixels, the time interval between laser pulses ( $\Delta t$ ) was either 30 or 50  $\mu\text{s}$ , depending on the test case.

The data was processed through a two-pass recursive algorithm using 50% grid spacing overlap. The first pass IW was  $64 \times 64$  pixels, and the resultant particle image displacement distance then applied to the second pass with an IW size of  $32 \times 32$  pixels. Signal-to-noise ratio is increased by offsetting the IW by the particle image displacement distance, as lost pairs due to in-plane motion are reduced. Validation of the vector fields generated was undertaken using a global velocity range test.

Data convergence was assessed using running averages of the turbulence intensity and velocity components. All results stabilised within the first 500 samples and did not show accumulative bias error, indicating sufficient convergence in the statistical parameters could be established from the number of vector fields recorded for each test case. To reduce measurement uncertainty 3000 image pairs were acquired for each test case. Presented in table 1 are the measurement uncertainties in the mean velocity and turbulence intensity components, non-dimensionalised by the rotor tip speed (20.73 m/s).

Mean Velocity Uncertainty	Turbulence Uncertainty (radial component)
$\pm 0.012$	$\pm 0.026$

Table 1. PIV measurement uncertainty in the mean velocity and radial turbulence intensity components.

## Results

For reasons of practicality, the deflectors were mounted directly to the ground board below the rotor. As a consequence the flow inboard of the rotor wake slipstream impinged upon the pylon connecting the deflector to the ground plane. Although it is assumed that this had a reasonably small effect on the results when considering the diameter of the pylon (26 mm) and the comparative strength of the rotor wake itself; the structure of the recirculating flow as presented includes additional interference effects not evident in the baseline case. It should also be noted that all data presented here form part of an ongoing study and as such represent preliminary findings.

Figure 9 and 10 show the PIV results for the phase-averaged velocity magnitude flow field of the rotor wake, non-dimensionalised by the rotor tip speed. The deflector radial velocities, measured using a pitot-static probe, were similarly non-dimensionalised to values of  $V_1=0.55$  and  $V_2=0.62$ . The height above the ground plane ( $z$ ), distance along the ground plane ( $x$ ) and radial distance ( $y$ ) have been non-dimensionalised by the rotor blade radius ( $R$ ). Figure 8 provides a pictorial representation of the axis system. The plot origin of figures 9 and 11 correspond to the intersection between the rotor hub centreline and the ground plane. For figure 10, the point (1,0) represents the centre point of the rotor hub.

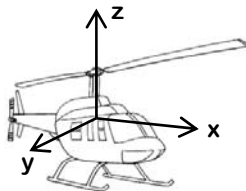


Figure 8. Axis system.

Figure 9(a) presents the baseline flow conditions, along with the flow field when the deflector is operating at  $V_1$  and  $V_2$ . The flow features of the baseline case are as expected [5, 6]. Although not visible as individual vortex cores in the mean flow field results, the blade tip vortices shed from the rotor are convected toward the ground, forming a slipstream. The velocity of the slipstream increases to a maximum as the wake contracts. The wake then

expands radially as the slipstream nears the ground plane. It should be noted that this expansion occurs more rapidly IGE when compared to operations out of ground effect. As a result of interaction with the ground plane and vortex merging [5] the region of slipstream flow near the ground shows increased velocity. A recirculation zone is also created near the centre of the rotor, and it is the change to this flow feature which will be used to quantitatively assess the effect of the flow deflectors.

Introducing the flow deflector, as per figures 9(b) and 9(c), has a clear effect of increasing the maximum velocity of the slipstream, which is to be expected. Of more interest to this investigation is the effect on the geometry of both the rotor wake slipstream and the flow field beneath the rotor hub. With the deflector installed the recirculation zone inboard of the slipstream boundary increases significantly in velocity.

With the deflector at  $V_1$  the centre of inboard recirculation zone is moved outboard by 42%, increasing to 54% at  $V_2$ . In the vertical direction the recirculation centre-point moves closer to the rotor by approximately 30% for both  $V_1$  and  $V_2$ .

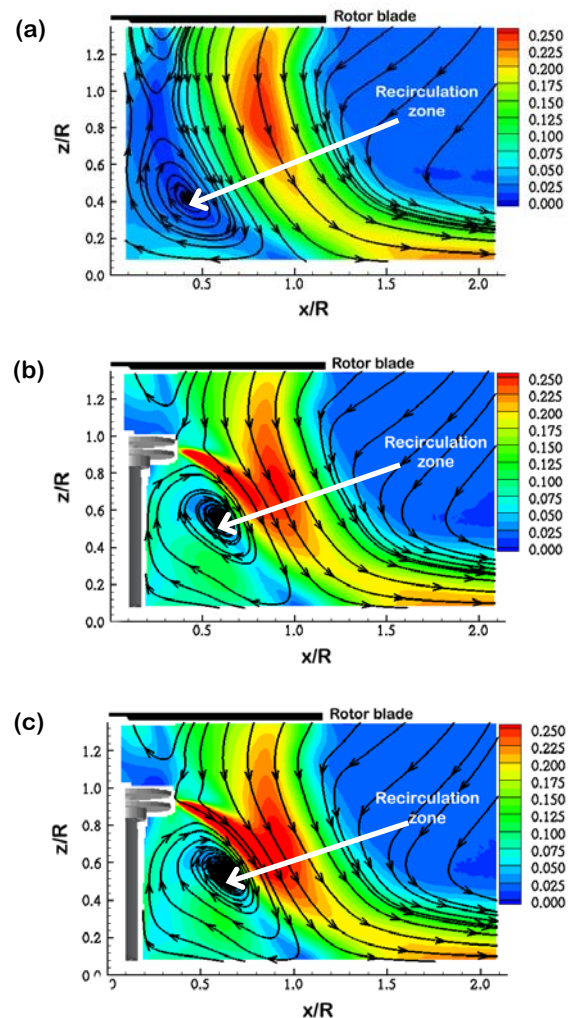


Figure 9. Non-dimensionalised rotor wake mean velocity magnitude contour plots. (a) Baseline, (b) Deflector at  $V_1$ , (c) Deflector at  $V_2$

The changes to the flow structure inboard of the rotor wake slipstream are also evident when considering the results shown in figure 10. It should be noted that the region of interest shown in these images provides a view in line with the top plate of the deflector, and as such shows the mean flow at a wake age several revolutions after the vortices were originally shed from the rotor blades. For any given radial plane within the rotor wake, the

mean velocity across the rotor disk is expected to fluctuate due to the passage of the vortex core. As shown in figure 10(a) the contraction and increased velocity of the rotor wake on the left hand side of the image indicates the movement of the vortex core through the plane. In addition, the region of wake inboard of the slipstream boundary shows the lower velocity of the recirculation zone.

With the deflector activated, it is much more difficult to identify the inner boundary of the rotor wake slipstream, although the lower velocity of the recirculation zone is still evident. Construction of the deflector resulted in an asymmetric jet flow field around the periphery of the outlet due to the location of the fasteners connecting the two plates, and this is reflected in figure 10(b). A secondary zone of low velocity is also evident below the peak jet flow on the lower right hand side of the image. Although two recirculation zones are expected to be observed inboard of the rotor slipstream [9], insufficient data was gathered during the experiment to determine whether the deflector introduced additional regions of recirculation as a result of the asymmetric jet flow.

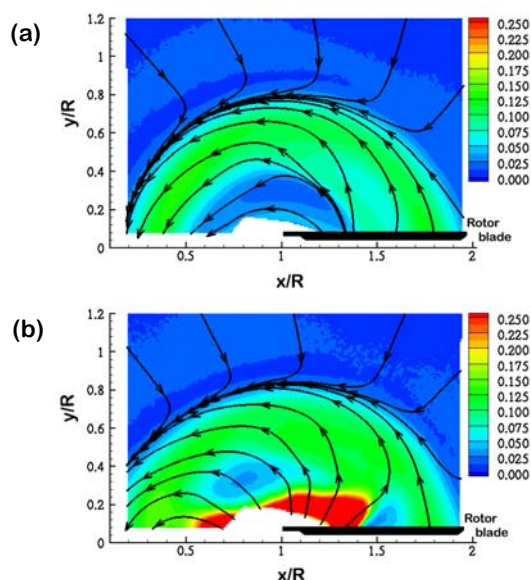


Figure 10. Non-dimensional plan view rotor wake mean velocity magnitude contour plots. a) Baseline, (b) Deflector at  $V_2$

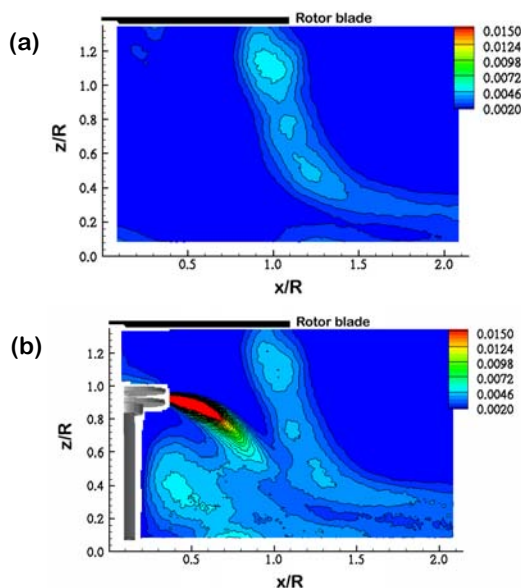


Figure 11. Non-dimensional rotor wake turbulence intensity contour plot, radial-component. (a) Baseline and (b) Deflector at  $V_2$

Figure 11 shows the PIV results for the phase-averaged turbulence intensity component of the rotor wake with the deflector operating at  $V_2$ . As expected, the baseline case shows the highest turbulence intensity at the location of the blade tip vortices. Introducing deflector peripheral jet flow to the rotor wake increased the turbulence of the flow both in the rotor slipstream and in the region beneath the rotor hub.

## Concluding Remarks

The active deflector had the desired effect on the rotor wake flow field, namely moving the slipstream boundary away from the rotor centreline, however, the addition of the jet flow significantly energised the flow in the region inboard of the slipstream boundary. Ideally the rotor wake should be altered in such a way so as to minimise the amount of flow recirculating past the cockpit, which is within the region inboard of the rotor wake slipstream boundary. To this end it is not yet possible to conclude whether or not the deflector tested in this case is suitable for the mitigation of brownout flow conditions, however, the experimental concept shows promise for further investigation.

## Acknowledgments

The authors wish to gratefully acknowledge the assistance of the following people; Dr. Matteo Giacobello and Dr. Ronny Widjaja for their advice and support during testing; for their technical support thanks to Paul Jacquemin, John Clayton, Chris Rider, Brett Lemke, and Paul Zavalis; and for photography support thanks to Brian Crowley and Marree Dixon.

## References

- [1] Curtiss Jr., H. C., Sun, M., Putman, W. F. & Hanker Jr., E. J., Rotor Aerodynamics in Ground Effect at Low Advance Ratios. *Journal of the American Helicopter Society* **29** (1) 1984, 48-55.
- [2] D'Andrea, A., Numerical Analysis of Unsteady Vortical Flows Generated by a Rotorcraft Operating on Ground: A First Assessment of Helicopter Brownout. In: *AHS International 65th Annual Forum*, American Helicopter Society, 2009, 1854-1877.
- [3] Hayden, J. S., Effect of the Ground on Helicopter Hovering Power Required. In: *AHS International 32nd Annual Forum*, American Helicopter Society, 1976.
- [4] Johnson, B., Leishman, J. G. & Sydney, A., Investigation of Sediment Entrainment in Brownout Using High-Speed Particle Image Velocimetry. In: *AHS International 65th Annual Forum*, American Helicopter Society, 2009, 1814-1837.
- [5] Lee, T. E., Leishman, J. G. & Ramasamy, M., Fluid Dynamics of Interacting Blade Tip Vortices With a Ground Plane. In: *AHS International 64th Annual Forum*, American Helicopter Society, 2008, 1231-1248.
- [6] Leishman, J. G., *Principles of Helicopter Aerodynamics*. ed. ed. Vol., Cambridge University Press, 2006.
- [7] Light, J. S., Tip Vortex Geometry of a Hovering Helicopter Rotor in Ground Effect. *Journal of the American Helicopter Society* **38** (2) 1993, 34-42.
- [8] Phillips, C., Kim, H. W. & Brown, R. E., Helicopter Brownout - Can it be Modelled? *The Aeronautical Journal* **115** (1164) 2011, 123-133.
- [9] Prouty, R. W., *Helicopter Aerodynamics*. ed. ed. Vol., PJS Publications, 1985.
- [10] Whitehouse, G. R., Wachspress, D. A., Quackenbush, R. R. & Keller, J. D., Exploring Aerodynamic Methods for Mitigating Brownout. In: *AHS International 65th Annual Forum*, American Helicopter Society, 2009, 1838-1853.
- [11] Williams, M. J. & Reddy, K. R., Description of a Simple Rotor Test Rig and Wake Studies. In: *Fourth Asian Congress of Fluid Mechanics*, 1989, G41-G44.